Journal of ELECTRONIC MATERIALS, Vol. 44, No. 4, 2015
DOI: 10.1007/s11664-015-3639-2

Effect of Thickness on Surface Morphology of Silver Nanoparticle Layer During Furnace Sintering

YOON JAE MOON,[1,2] HEUISEOK KANG,[2] KYUNGTAE KANG,[2] SEUNG-JAE MOON,[1,3] and JUN YOUNG HWANG[2,4]

1.—Department of Mechanical Engineering, Hanyang University, Seoul 133-791, Republic of Korea. 2.—Korea Institute of Industrial Technology, Ansan, 426-173, Republic of Korea. 3.—e-mail: smoon@hanyang.ac.kr. 4.—e-mail: jyhwang@kitech.re.kr.

In printed electronics applications, specific resistances of conductive lines are critical to the performance of the devices. The specific resistance of a silver (Ag) nanoparticle electrode is affected by surface morphology of the layered nanoparticles which were sintered by the heat treatment after printing. In this work, the relationship between surface morphology and specific resistance was investigated with various sintering temperatures and various layer thicknesses of Ag nanoparticle ink. Ag nanoparticles with an average size of approximately 50 nm were spin-coated on Eagle XG glass substrates with various spin speed to change the layer thickness of Ag nanoparticles from 200 nm to 900 nm. Coated Ag nanoparticle layers were heated from 150°C to 450°C for 30 min in a furnace. The result showed that higher sintering temperature produces larger grains in an Ag layer and decreases specific resistance of the layer, but that the maximum allowable heating temperature is limited by the thickness of the layer. When grain size exceeded the thickness of the layer, the morphology of the Ag nanoparticles changed to submicron-sized islands and the Ag layers did not have electrical conductivity any more.

Key words: Silver nanoparticle, spin-coating, grain, furnace sintering

INTRODUCTION

Recently, interest has grown in printed electronics because printing methods can replace the traditional silicon-based techniques, which require many processing steps such as vacuum deposition, photolithography, and etching. Printing offers the potential for low-cost, large-area electronics for displays, sensors, radiofrequency identification, and polymer micro-electromechanical systems.[1–6] Crucial components of printed electronics include conductive lines and electrodes using metal nanoparticle inks. Gold nanoparticles have been used for conductive materials due to their high electrical conductivity and thermal stability. However, these particles are not widely applied in the industry due to cost. Replacement by copper nanoparticles is an alternative, as copper has been recently used in metal-wiring material in a semiconductor foundry by the introduction of the chemical–mechanical polishing Damascene process. However, printed copper nanoparticles oxidize rapidly under air conditions. Therefore, silver (Ag) nanoparticle inks are currently the material of choice for printing electrical conductive patterns in printed electronics.[7–9]

Electrodes with high electrical conductivity are advantageous because they can reduce not only energy loss but also the resistance–capacitance time delay to achieve high-speed circuits. In general, printed Ag nanoparticle electrodes have higher electrical conductivity when they are sintered at higher temperature after printing, because elevated temperature causes the metal nanoparticles to agglomerate having enhanced connectivity among the nanoparticles.[10–12] However, unfortunately, the increase of the electrical conductivity with elevating sintering temperature has limitations. Further

(Received July 23, 2014; accepted January 8, 2015; published online January 30, 2015)

heating results in the loss of electrical conductivity due to the formation of too large Ag agglomeration and broken connectivity.[13–16] The limitation of sintering temperature could be critical to some application where high temperature processes should be followed up. For example, printing of oxide semiconductor thin film transistors (TFTs) might need high-temperature treatments at 300–600°C for metal oxides, and the already printed bottom electrodes will also suffer the high temperature.[17,18]

In this background, the study of Perelaer et al. is remarkable as it reported that no loss of conductivity was observed until heating inkjet-printed silver lines having a thickness of approximately 6 μm to 650°C for five times, while the single printed lines having a thickness of 1.5 μm had minimum resistance at 325°C.[16] They also commented that the reason for the different behavior of the resistance with increasing temperature could be due to the formation of cracks which would be more apt to occur in the lines having a smaller thickness.[16] However, further evidence on the effect of layer thickness on the sintering characteristics of Ag nanoparticles has not yet been revealed, even though controlling the maximum allowable temperature of printed Ag nanoparticles by changing the layer thickness would be attractive. Motivated by this, the variations of surface morphology and specific resistance were experimentally investigated with various sintering temperatures and layer thicknesses of Ag nanoparticle ink on a glass substrate.

EXPERIMENTAL

The ink used (ANP, DGP-40LT-15C) contains 31 wt.% spherical Ag nanoparticles, having an average diameter of 50 nm, dispersed in triethylene glycol monoethyl ether (TGME). Suggested sintering conditions were 30–60 min at 150°C. Either inkjet printing or spin coating was used for line-patterning or film-coating of the Ag ink, respectively. The drop-on-demand (DOD) inkjet printing device (Dimatix, DMP-2381) consists of a cartridge-type jetting head, a 2-D traverse stage, a monitoring camera, and a working bed. It generates a series of droplets with volumes of approximately 6.5 pl and a drop diameter of 23 μm. Ink was printed on an Eagle XG glass substrate with a thickness of 500 μm. Before printing, glass substrates were cleaned in an ultrasonic cleaner by using acetone and isopropyl alcohol. The substrates were dried in an oven at 150°C for 15 min. The printed Ag line was 3 mm long and 140 μm wide. Contacting pads are printed at both ends of the line for ohmmeter probes. To lower the electrical resistance, the substrate was heated to 250°C for 30 min before printing the line. Spin coating was used at various speeds to vary the thickness of the Ag layer. The glass (Eagle XG) substrate of 24 mm by 24 mm was rotated at speeds of 500 rpm, 1000 rpm, and 2000 rpm. After spin coating, samples were dried at 50°C for 30 min. The printed and spin-coated samples were sintered in a furnace at various temperatures from 150°C to 450°C with an interval of 50°C. Sintering time was set to 30 min because a previous study revealed that the specific resistance of the adopted Ag ink changes little after 20 min of heating in a furnace.[19]

Cross-sectional thickness profiles of inkjet-printed lines and spin-coated layers were measured before and after sintering using an Alpha-Step (KLA-Tencor). Also, the thickness of the spin-coated layer was obtained by averaging the cross-sectional thickness profiles at 3 or 4 positions around the center of the substrate, each of which had a scan length of 2.5 mm. The electrical resistance of a line was measured by a 1160 probe station (Signatone) and a 433B milliohmmeter (Agilent). Sheet resistance of spin-coated samples was measured using a M4P 302-system four-point probe (MS TECH) and multimeter (Fluke 8845A). The specific resistance was calculated by multiplying the electrical resistance of the inkjet-printed lines by the cross-sectional area and dividing it by length, and the specific resistance of the spin-coated samples was calculated by multiplying the sheet resistance by the thickness. XRD was performed to confirm the oxidation of Ag with temperature. Specific resistance was related to the morphology change of the printed metal nanoparticles. To examine the morphology of the printed metal nanoparticles, a SU8000 FESEM (Hitachi) was used. Grain size was measured from the FESEM images: the number of grains was counted along the diagonal line on a FESEM image, and then the average grain size was calculated by dividing the number of grains by the length of the diagonal line.

RESULTS AND DISCUSSION

Figure 1 shows the specific resistance of inkjet-printed silver nanoparticles as a function of furnace

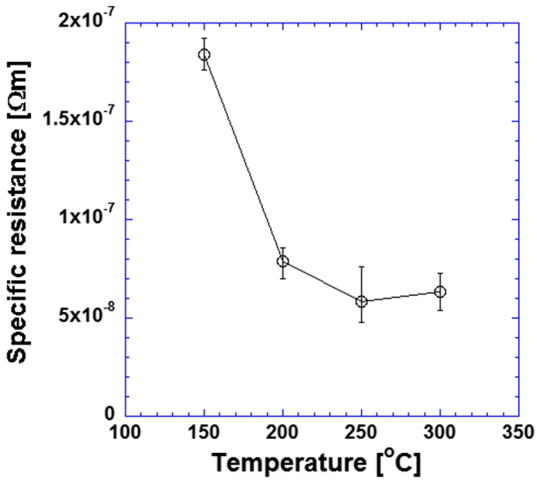

Fig. 1. The change in specific resistance of inkjet-printed Ag nanoparticles treated at various temperatures for 30 min.

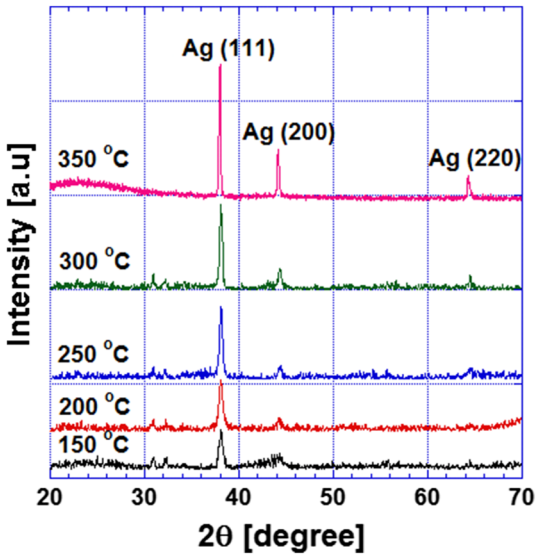

Fig. 2. XRD results of Ag nanoparticles treated at various temperatures for 30 min.

temperature. The specific resistance was measured at room temperature after the 30-min furnace treatment. Before furnace sintering, electrical resistance was more than 100 MΩ. The specific resistance of the inkjet-printed silver nanoparticles sintered at 150°C was 1.84×10^{-7} Ω m, which is 11.5 times higher than that of bulk Ag (1.6×10^{-8} Ω m). The minimum specific resistance was obtained at 250°C, 5.8×10^{-8} Ω m. This is 3.7 times higher than that of bulk Ag. When Ag nanoparticles were further heated at a higher temperature, the specific resistance began to increase and electrical resistance exceeded the multimeter's measuring limit of 100 MΩ at 350°C. This nonlinear variation of the specific resistance of Ag nanoparticle layer agrees well with previous studies.[13–16]

To examine the reason of this nonlinear variation of electrical conductivity, XRD measurements were first carried out and the possible oxidation of Ag nanoparticles were checked. As shown in Fig. 2, Ag oxide was not formed in the temperature range

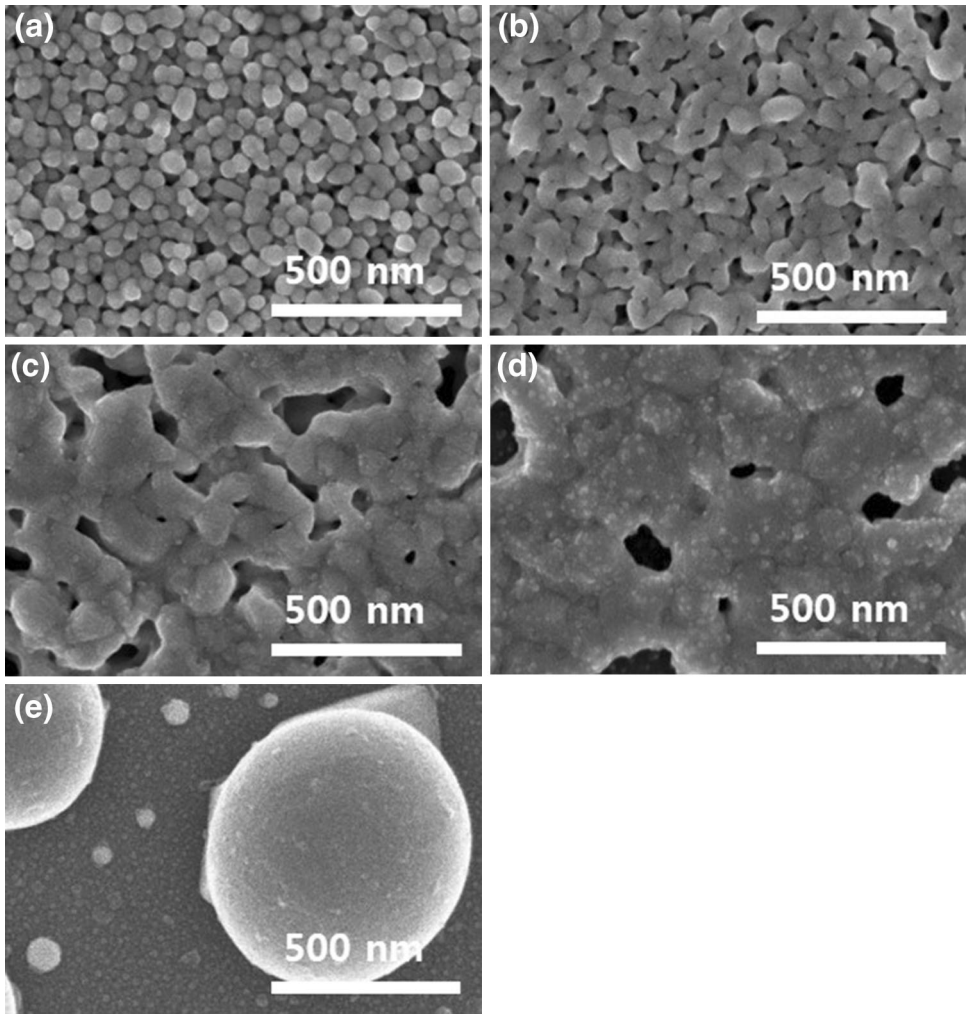

Fig. 3. FESEM images of inkjet-printed Ag nanoparticles treated at various temperatures: (a) 150°C, (b) 200°C, (c) 250°C, (d) 300°C, and (e) 350°C.

studied, which is in agreement with other results in air.[20,21] XRD analysis probed the formation of well-crystallized silver. The (1 1 1), (2 0 0), and (2 2 0) corresponded to the face-centered cubic structure of the metallic silver.

The next approach of the examination was to obtain FESEM images to observe the formation of the neck connectivity of the sintered ink, which is expected to be crucial in varying the specific resistance. Figure 3 shows surface images of Ag nanoparticles after sintering. At 150°C, the initial shape of the particles was maintained and a neck was formed. Due to the neck formation between particles, the specific resistance was reduced. At 200°C, silver nanoparticles were completely merged. In this temperature regime, the mechanism for sintering is surface energy reduction.[10–12]

In high-temperature regimes, such as those depicted in Fig. 3b–e, the silver nanoparticles coalesce into larger particles with increasing temperature by grain boundary diffusion and lattice diffusion triggered by Ostwald ripening.[22,23] Then, the surface of the ink provides more effective transport paths for electron flow than in the lower sintering temperature case. Above 250°C, grain and pore growth begins to occur. Large pores existed after sintering at 300°C. Due to the formation of large pores, specific resistance did not decrease. At 350°C, the connection among silver nanoparticles was completely broken and submicron-sized large silver islands having diameters of 500 nm or larger were formed. Therefore, the Ag layer became to lose its electrical conductivity.

Figure 4 shows a cross-section of the printed ink line measured by a surface profiler. The cross-section of the ink line was selected at the middle point of the printed line. Figure 4a represents the cross-sectional shape of the inkjet-printed line. This shows a coffee ring effect, that is, the thickness of the center is lower than that of the edges. The thickness of the center and edges were approximately 200 nm and 340 nm, respectively. Figure 4b shows the average grain size and thickness of inkjet-printed lines as a function of temperature. With increasing temperature, grain size increased and approached the thickness of the line. Grain size was similar to the thickness of the center of the line at 300°C. At 350°C, the grain size and the line thickness could not be measured because of the formation of silver islands as shown in Fig. 3e, whereas the diameters of the islands were generally larger than 500 nm, which value could correspond to the maximum thickness of the line.

The above results imply that the breaking of the Ag nanoparticle layers into Ag islands has a strong relationship with the increase of grain size relative to the thickness of the layer. To study the effect of the grain size relative to the layer thickness on the change in specific resistance and morphology, Ag nanoparticle ink was spin-coated with various spin speeds and then sintered at various temperatures. Figure 5 shows the variation in average thickness of the coated Ag layer with respect to rotational speed of the spin coating, which shows an almost linear decrease of the thickness with the spin speed. Each

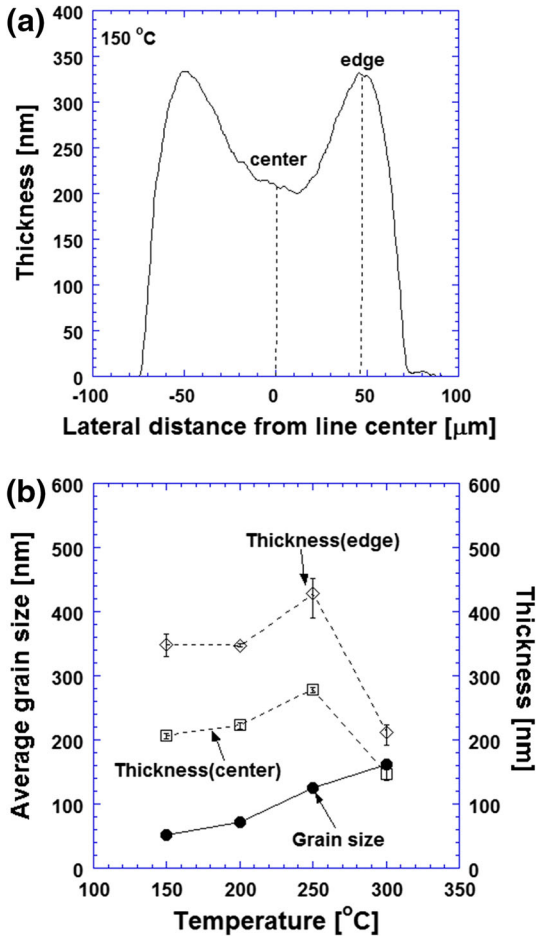

Fig. 4. (a) Cross-section of inkjet-printed lines after sintering at 150°C for 30 min and (b) average grain size and thickness of inkjet-printed lines with various temperatures.

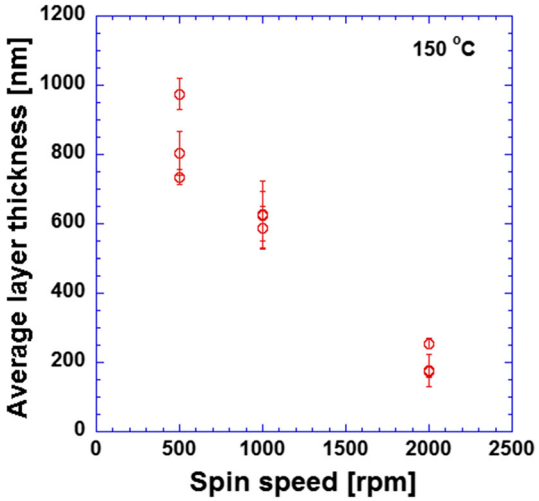

Fig. 5. Average thickness of coated Ag layer as a function of rotational speed of the spin coating.

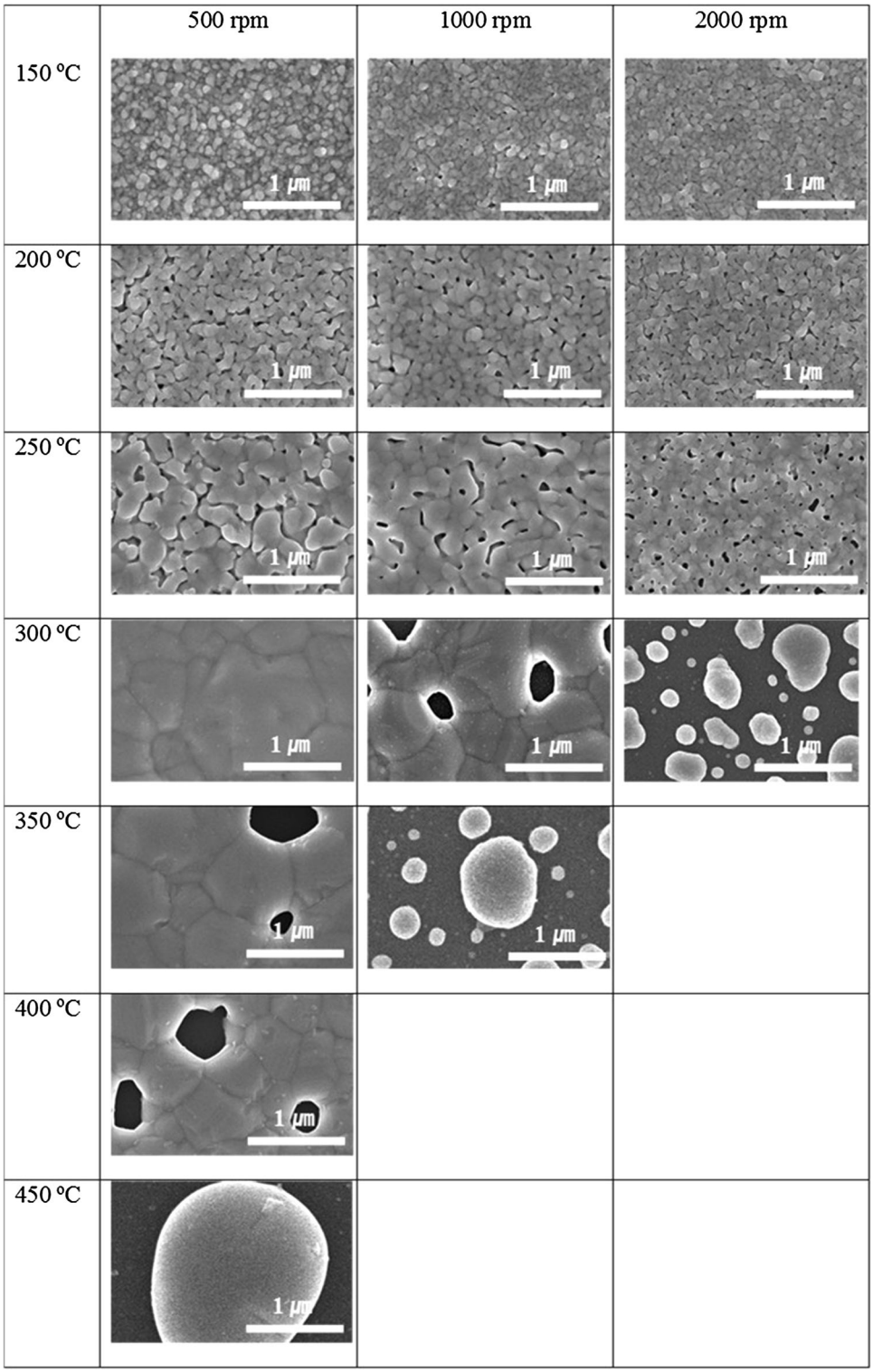

Fig. 6. FESEM images of spin-coated Ag nanoparticles with various spin speeds and temperatures.

symbol in Fig. 5 represents the average thickness of a spin-coated layer obtained by averaging cross-sectional thickness profiles for 2500-μm scan length. The standard deviation of each scan was in the order of 10%, shown as error bars in the figure.

Figure 6 shows FESEM images of the layer surfaces. It was commonly observed for the Ag nanoparticles coated with various spin speeds that they were sintered to make larger grains at higher temperature until they formed islands. It was also

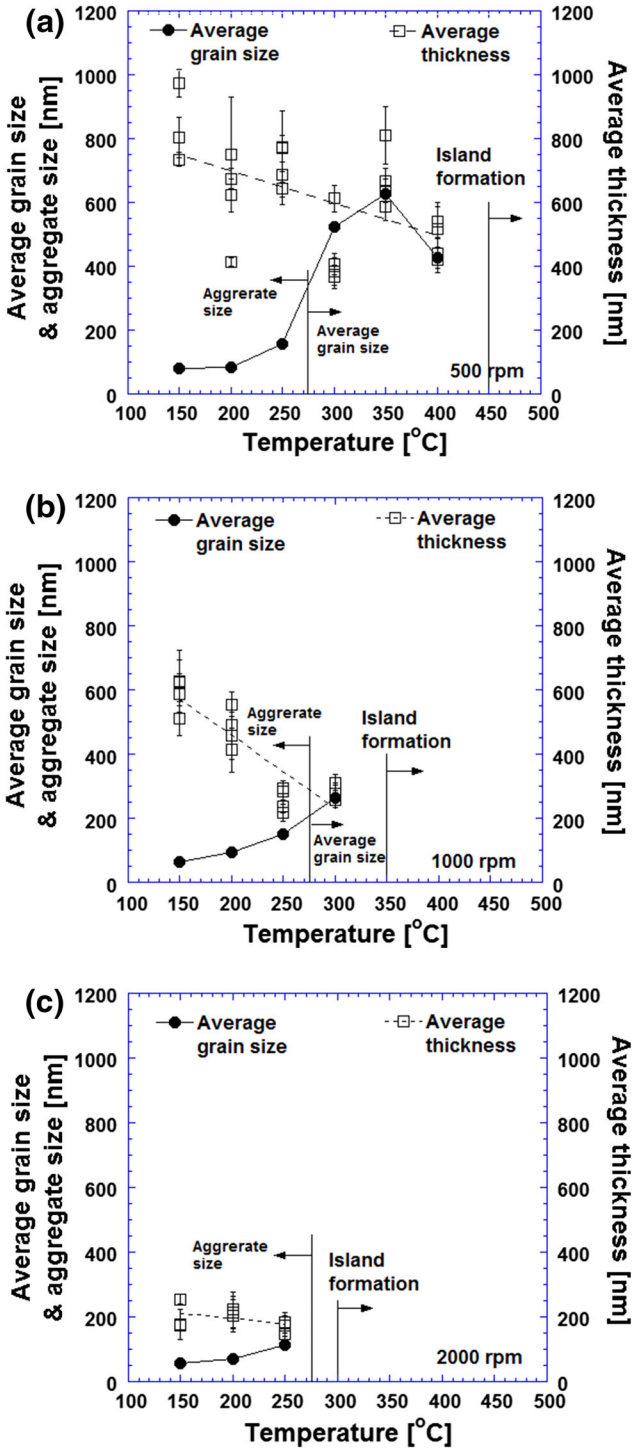

Fig. 7. The change of average grain size and average thickness with temperature: (a) 500 rpm, (b) 1000 rpm, (c) 2000 rpm.

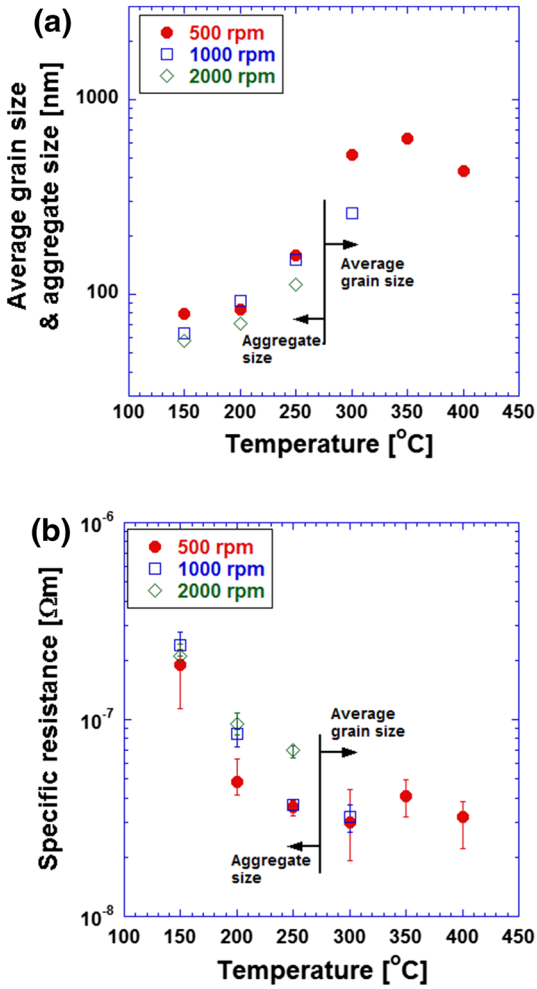

Fig. 8. The temperature-dependent variations of (a) average grain size and (b) specific resistances for different spin speeds.

commonly observed that large pores began to be noticeable just before the formation of Ag islands. However, it is clearly shown that the temperature at which Ag islands formed increased with decreasing spin speed or increasing thickness: 300°C at 2000 rpm, 350°C at 1000 rpm, and 450°C at 500 rpm. As a result, the island size at the formation temperature and the grain size just before the formation also increased with decreasing spin speed or increasing thickness, as shown in the images.

Figure 7 shows the change in average grain size and aggregate size and average thickness with temperatures and spin speeds. Aggregation is a procedure that pre-sintered nanoparticles are bonded together by solid necks of significant strength such as metallic force. Before the grain growth, the boundary between particles cannot be clearly identified in the FESEM images. As the grain boundary can be clearly seen in the FESEM images, it is defined as grain size. As shown in Fig. 6, the surface morphology of Ag nanoparticles to 250°C was similar to that of the final aggregation of the nanoparticles.[24] Particle size to 250°C is defined as the aggregate size. Above 300°C, grain growth occurred. So, the average grain size could be measured from FESEM images above 300°C. The dashed line represents the linear fit of the average thickness, which decreases slightly with temperature possibly due to

decreasing porosity in the layer with the progress of sintering. In Fig. 7, with increasing temperature, grain size approached the thickness of the film. Aggregate size slowly increased from 50 nm to 150 nm until 250°C in all cases. Above 250°C, the grain size of the Ag nanoparticles coated at 500 rpm abruptly increased above 500 nm. As a result of the increase in the grain size and the decrease in the thickness with temperature, the grain size became similar to the thickness of the layer at 400°C, 300°C, and 250°C for 500 rpm, 1000 rpm, and 2000 rpm, respectively. Finally, above those temperatures, Ag islands were formed in the Ag layers and the layers did not have any meaningful electrical conductivity.

As soon as the particles were placed in contact with each other, necks formed between the particles. The necks grow by several different mechanisms including surface diffusion, lattice diffusion from the surface, vapor transport, grain boundary diffusion, and lattice diffusion from the grain boundary accompanied by plastic flow.[25,26] It has been reported that surface and grain boundary diffusions were more significant transport processes in sintering of metal nanoparticles at relatively low temperatures.[21] In contrast, the volumetric transport processes such as lattice diffusions become active at relatively higher temperatures.[10–12] When the grains have already grown to reach the surface of the layers, and they are driven to keep growing by the volumetric transport processes, the grains could not grow together any further but separated into islands. Therefore, at the breaking temperature, the originally porous Ag layer with a closely packed structure of nanoparticles changes to a discontinuous layer consisting of solid islands and surrounding voids.

The effect of the layer thickness, however, was limited to the island formation phenomenon. Figure 8 shows the change in the average grain size and specific resistance with various temperatures and spin speeds. With the increase of sintering temperature to 300°C, the grain size increased and specific resistance decreased exponentially, where the difference in the spin speeds did not affect the overall trends of these variations very much. The noticeable isolations from the trends for both the grain size and specific resistance were observed only near the breaking temperature. Without interruption of the island formation, the grain sizes grew to approximately 650 nm and the specific resistance of the silver layer spin-coated at 500 rpm decreased to 3.0×10^{-8} Ω m at 300°C, due to the decrease of the grain boundary area which is operated as electron-scattering sites. Above 300°C, the variations of the grain sizes and specific resistance diminished, not having clear directions.

CONCLUSION

The morphology of Ag nanoparticle ink printed or coated with various thicknesses and sintered at various temperatures was experimentally investigated to show that the high-temperature stability of the Ag nanoparticle layer is directly affected by the layer thickness. At the beginning of the temperature elevation, the agglomeration of the Ag nanoparticles and growth of the grains enhanced the electrical conductivity of the Ag layer. When the temperature increased further, the sintered Ag layer was broken into a separated array of submicron islands and lost its electrical conductivity. This result showed that the breaking temperature of the sintered layer into the islands increases with the thickness of the layer. The experimental observation revealed that, for a thin Ag nanoparticle layer having submicron thickness, the breaking of the sintered layer occurs when the grains grow to the thickness of the layer, because growth further than the thickness drives a grain to absorb the adjacent grains to be detached from the surrounding layer. As a result, the thicker layer enabled the enduring of higher temperatures without breaking and, therefore, to reach higher electric conductivity of the layer.

ACKNOWLEDGEMENT

This work was supported by a grant from the Industrial Source Technology Development Program (Grant 10041041) of the Ministry of Trade, Industry and Energy of Korea.

REFERENCES

1. J.W. Kang, W.I. Jeong, J.J. Kim, H.K. Kim, D.G. Kim, and G.H. Lee, High-performance flexible organic light-emitting diodes using amorphous indium zinc oxide anode. *Electrochem. Solid-State Lett.* 10, 75 (2007).
2. L. Hou, F. Huang, W. Zeng, J. Peng, and Y. Cao, High-efficiency inverted top-emitting polymer light-emitting diodes. *Appl. Phys. Lett.* 87, 153509 (2005).
3. V. Shamanna, S. Das, Z. Celik-Butler, and K.L. Lawrence, Micromachined integrated pressure–thermal sensors on flexible substrates. *J. Micromech. Microeng.* 16, 1984 (2006).
4. F. Jiang, G.B. Lee, Y.C. Tai, and C.M. Ho, A flexible micromachine-based shear-stress sensor array and its application to separation-point detection. *Sens. Actuators A* 79, 194 (2000).
5. S.A. Day, D.P. Butler, and Z. Celik-Bulter, Micromachined infrared bolometers on flexible polyimide substrates. *Sens. Actuators A* 118, 49 (2005).
6. S. Tung, S.R. Witherspoon, L.A. Roe, A. Silano, D.P. Maynard, and N. Ferraro, AMEMS-based flexible sensor and actuator system for space inflatable structures. *Smart Mater. Struct.* 10, 1230 (2001).
7. K.J. Lee, B.H. Jun, T.H. Kim, and J. Joung, Direct synthesis and inkjetting of silver nanocrystals toward printed electronics. *Nanotechnology* 17, 2424 (2006).
8. D. Kim, S. Jeong, B.K. Park, and J. Moon, Direct writing of silver conductive patterns: Improvement of film morphology and conductance by controlling solvent compositions. *Appl. Phys. Lett.* 89, 264101 (2006).
9. T.H.J. Van Osch, J. Perelaer, A.W.M. De Laat, and U.S. Schubert, Inkjet printing of narrow conductive tracks on untreated polymeric substrates. *Adv. Mater.* 20, 343 (2008).
10. W.D. Kingery, H.K. Bowen, and D.R. Uhlmann, *Introduction to Ceramics* (New York: Wiley, 1976).
11. F.F. Lange, Sinterability of agglomerated powders. *J. Am. Ceram. Soc.* 67, 83 (1984).

12. C.J. Brinker and G.W. Scherer, *Sol–Gel Science* (San Diego, CA: Academic, 1990).
13. K.S. Chou, K.C. Huang, and H.H. Lee, Fabrication and sintering effect on the morphologies and conductivity of nano-Ag particle films by spin coating method. *Nanotechnology* 16, 779 (2005).
14. J.W. Park and S.G. Baek, Thermal behavior of direct-printed lines of silver nanoparticles. *Scr. Mater.* 55, 1139 (2006).
15. Y.J. Moon, H. Kang, K. Kang, J.Y. Hwang, J.H. Lee, and S.J. Moon, Effect of laser intensity on the characteristics of inkjet-printed silver nanoparticles during continuous laser sintering. *J. Nanosci. Nanotechnol.* 14, 8631 (2014).
16. J. Perelaer, A.W.M. de Laat, C.E. Hendriks, and U.S. Schubert, Inkjet-printed silver tracks: low temperature curing and thermal stability investigation. *J. Mater. Chem.* 18, 3209 (2008).
17. B.J. Norris, J. Anderson, J.F. Wagner, and D.A. Keszler, *J. Phys. D.* 36, L105 (2003).
18. J.H. Lim, J.H. Shim, J.H. Choi, J.H. Joo, K. Park, H.S. Jeon, M.R. Moon, D.G. Jung, H.S. Kim, and H.J. Lee, Solution-processed InGaZnO-based thin film transistors for printed electronics applications. *Appl. Phys. Lett.* 95, 012108 (2009).
19. J.Y. Hwang and S.J. Moon, The characteristic variations of inkjet-printed silver nanoparticle ink during furnace sintering. *J. Nanosci. Nanotechnol.* 13, 6145 (2013).
20. K.S. Moon, H. Dong, R. Maric, S. Pothukuchi, A. Hurt, y. Li, and C.P. Wang, Thermal behavior of silver nanoparticles for low temperature interconnect applications. *J. Electron. Mater.* 34, 168 (2005).
21. J.S. Kang, J. Ryu, H.S. Kim, and H.T. Hahn, Sintering of inkjet printed silver nanoparticles at room temperature using intense pulsed light. *J. Electron. Mater.* 40, 2268 (2011).
22. P. Zeng, S. Zajac, P.C. Clapp, and J.A. Rifkin, Nanoparticle sintering simulations. *Mater. Sci. Eng. A* 252, 301 (1998).
23. M.J. Mayo, Processing of nanocrystalline ceramics from ultrafine particles. *Int. Mater. Rev.* 41, 85 (1996).
24. B. Ingham, T.H. Lim, C.J. Dotzler, A. Henning, M.F. Toney, and R.D. Tilley, How nanoparticles coalesce: an in situ study of Au nanoparticle aggregation and grain growth. *Chem. Mater.* 23, 3312 (2011).
25. D.W. Richerson, *Modern Ceramic Engineering: Properties, Processing and Use in Design*, 2nd ed. (New York: Marcel Dekker, 1992).
26. M.N. Rahaman, *Ceramic Processing and Sintering*, 2nd ed. (New York: Marcel Dekker, 2003).